Correspondence and
requests for materials
should be addressed to
Z.L.L. (zl-liu@imre.a-
star.edu.sg) or W.C.
(phycw@nus.edu.sg)

Porous Perovskite LaNiO₃ Nanocubes as Cathode Catalysts for Li-O₂ Batteries with Low Charge Potential

Jian Zhang[1], Yubao Zhao[1], Xiao Zhao[1], Zhaolin Liu[2] & Wei Chen[1,3,4]

[1]Department of Chemistry, National University of Singapore, 3 Science Drive 3, 117543, Singapore, [2]Institute of Materials Research and Engineering (IMRE), Agency of Science, Technology, and Research (A*STAR), 3 Research Link, Singapore 117602, Singapore, [3]Department of Physics, National University of Singapore, 2 Science Drive 3, 117542, Singapore, [4]National University of Singapore (Suzhou) Research Institute, Suzhou, China.

Developing efficient catalyst for oxygen evolution reaction (OER) is essential for rechargeable Li-O₂ battery. In our present work, porous LaNiO₃ nanocubes were employed as electrocatalyst in Li-O₂ battery cell. The as-prepared battery showed excellent charging performance with significantly reduced overpotential (3.40 V). The synergistic effect of porous structure, large specific surface area and high electrocatalytic activity of porous LaNiO₃ nanocubes ensured the Li-O₂ battery with enchanced capacity and good cycle stability. Furthermore, it was found that the lithium anode corrosion and cathode passivation were responsible for the capacity fading of Li-O₂ battery. Our results indicated that porous LaNiO₃ nanocubes represent a promising cathode catalyst for Li-O₂ battery.

Rechargeable lithium-oxygen batteries with remarkably high theoretical energy storage capacity have attracted significant attention due to their potential applications in electric vehicles[1–7]. It is predicted that the energy density of the Li-O₂ battery is around 10 times higher than that of the current Li-ion battery[1,4]. A typical rechargeable Li-O₂ battery cell comprises porous cathode, lithium anode, separator and Li⁺ conducting electrolyte. However, this system suffers from many challenges for practical applications, such as electrolyte instability, poor cycle stability and high overpotential[8–11]. All these problems are related to the sluggish oxygen evolution reaction (OER). The overpotential for charge process (i.e., OER) is up to 1.0–1.50 V, which is much higher than that for discharge process (0.30 V)[12]. To date, the most efficient OER catalysts are noble metals[13,14]. For example, Ru nanocrystal shows a good catalytic performance with a discharge-charge overpotential as low as about 0.37 V[15]. However, the scarcity and high cost of noble metals limit their large-scale applications. Therefore, it is highly desirable to develop non-precious metal catalysts for OER[16–22].

Perovskite oxides (ABO₃), which are widely used as catalysts for fuel cells and zinc-air batteries, recently have also been evaluated for Li-O₂ batteries[23–28]. Y. L. Zhao and his colleagues developed hierarchical mesoporous perovskite La₀.₅Sr₀.₅CoO₂.₉₁ nanowires and obtained high capacity of 11059 mAh g⁻¹ [29]. J. J. Xu et.al used perovskite-based porous La₀.₇₅Sr₀.₂₅MnO₃ nanotube as the cathode for Li-O₂ battery and cycled the battery over 124 cycles at a 1000 mAh g⁻¹ capacity limitation[30]. S. H. Yang and co-workers have systematically investigated the electrocatalytic activity of perovskite oxide through molecular orbital principle; they predicted that LaNiO₃ possessed unique intrinsic activity for both oxygen reduction reaction (ORR) and OER among the perovskite type oxides[31,32]. In addition, porous materials have been demonstrated to show extra advantage in Li-O₂ battery applications[17,29,30]. The porous structure can provide ideal pathway for oxygen transfer and electrolyte diffusion, as well as more catalytic active sites to promote the ORR and OER.

In this work, porous pervoskite LaNiO₃ nanocubes were synthesised and employed as the cathode catalyst for Li-O₂ battery. The as-prepared catalyst showed improved performance in both discharge and charge process. In particular, in charge process, the catalyst could significantly reduce the overpotential up to ~260 mV and ~350 mV compared with the LaNiO₃ particles and commercial Vulcan XC-72 carbon (VX-72) electrodes at the current density of 0.08 mA cm⁻². The charge voltage could be even decreased to 3.40 V at lower current density of 0.016 mA cm⁻². The Li-O₂ battery assembled by the porous LaNiO₃ nanocubes as cathode catalyst also showed enhanced capacity and good cycle stability.
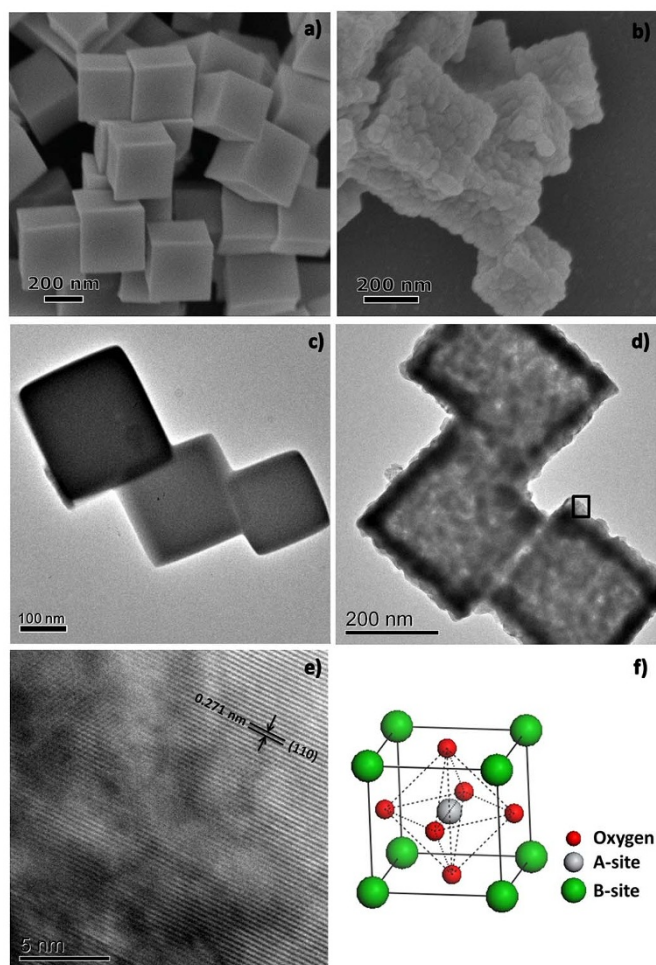
Figure 1 | SEM (a, b) and TEM (c, d) images of the obtained nanocube-like precursors before (a, c) and after (b, d) annealing, respectively; (e) High-resolution TEM image of porous $LaNiO_3$ nanocubes; (f) ABO_3 perovskite oxides structure.

Results

Synthesis and characterization of porous $LaNiO_3$ nanocubes. The nanocube-like precursors were synthesized *via* a modified hydrothermal process[33], with the pH value of 7.7 and the glycine to metal salt molar ratio of 3 : 1. Fig. 1a and 1c show the scanning electron microscopy (SEM) and transmission electron microscope (TEM) images of the as-prepared nanocube-like precursors. These precursors had smooth surfaces with the size about 250 nm. After annealing in O_2 at 650°C for 2 h, the surface of the annealed products became rough and rich porosity was created (Fig. 1b and 1d). At the same time, the original cubic shape was not significantly changed. As displayed in the high-resolution TEM image in Fig. 1e, the distance of the adjacent fringes was 0.271 nm, corresponding to the lattice spacing of the (110) plane of perovskite-type $LaNiO_3$. The X-ray diffraction (XRD) pattern (Fig. 2a) revealed that the annealed products were perovskite-type $LaNiO_3$ (PDF#34-1028) without any La_2O_3 or NiO related phase. This indicates that the nanocube-like precursors had completely transformed into $LaNiO_3$ after the 650°C annealing. The BET specific surface area of the annealed products was 35.8 $m^2 g^{-1}$ (Fig. 2b). It was nearly 10 times as high as that of the $LaNiO_3$ particles prepared without glycine (Fig. S1). The average pore diameter of the porous $LaNiO_3$ nanocubes was ~30 nm (Inset in Fig. 2b). However, without glycine, the nanocubic structure and rich porosity could not be obtained (Fig. S1, S2). Herein, glycine not only acted as a pore-forming agent but

also a shape-control agent in the formation of porous nanocubic structure[34,35].

Electrochemical Measurements and Li-O_2 Battery Test. The electrochemical performance of the porous $LaNiO_3$ nanocubes catalyst was measured by the galvanostatic charge-discharge measurements in a modified Swagelok Li-O_2 battery cell using 1 M lithium trifluoromethanesulfonate/tetraethylene glycol dimethyl ether (LiCF$_3$SO$_3$/TEGDME) as the electrolyte. Reference cathodes made by either $LaNiO_3$ particles or commercial VX-72 carbon were employed for comparison. Fig. 3a shows the first discharge-charge profiles of the Li-O_2 cells with porous $LaNiO_3$ nanocubes, $LaNiO_3$ particles and VX-72 carbon electrodes at a current density of 0.08 mA cm^{-2}. The discharge capacity of the battery cell with porous $LaNiO_3$ nanocubes electrode was up to 3407 mAh g^{-1}, which was higher than that of the $LaNiO_3$ particles (2639 mAh g^{-1}) and VX-72 carbon (2545 mAh g^{-1}) electrodes based batteries. The enhanced discharge capacity of the porous $LaNiO_3$ nanocubes electrode was attributed to their high catalytic activity to promote the ORR.

As shown in Fig. 3a, the porous $LaNiO_3$ nanocubes catalyst possessed excellent OER performance with the charge voltage plateau at about 3.87 V, which was lower than that of the $LaNiO_3$ particles and VX-72 carbon catalysts by ~260 mV and ~350 mV, respectively. In order to further investigate the OER performance of porous $LaNiO_3$ nanocubes electrode, galvanostatic discharge-charge measurements at 0.16, 0.04 and 0.016 mA cm^{-2} were also performed (Fig. 3b). When the current density was 0.016 mA cm^{-2}, the charge plateau was lower to 3.40 V. To our knowledge, this value was one of the lowest charge potentials among the reported metal oxide catalysts[36–38]. Even at a higher current density (0.16 mA cm^{-2}), the charge plateau only increased to 4.00 V, which was also lower than that of other metal oxide catalysts at the same current density[17,30]. These results demonstrate that the porous $LaNiO_3$ nanocubes catalyst possesses excellent OER performance under a wide range of current densities. Electrochemical measurement in non-aqueous electrolyte system was carried out to confirm the high OER performance of porous $LaNiO_3$ nanocubes catslyst. As shown in chronoamperometry process and Linear sweep voltammetry (LSV) measurement (Fig. 3c and 3d), the porous $LaNiO_3$ nanocubes catalyst showed higher response current density compared with $LaNiO_3$ particle and VX-72 carbon catalysts, suggesting the promotion effects of porous $LaNiO_3$ nanocubes catalyst on both ORR and OER[36,39,40]. The LSV measurement showed no obvious difference of the onset potential among porous $LaNiO_3$ nanocubes, $LaNiO_3$ particles and VX-72 carbon electrodes, which is consistent with previous reports[36,41].

Discussion

Our experimental results showed that the porous $LaNiO_3$ nanocubes catalyst exhibited superior ORR and OER activity towards the formation and decomposition of discharge products, resulting in a low overpotential of the battery cell. The good catalytic activity of the porous $LaNiO_3$ nanocubes electrode could be attributed to the intrinsic properties of perovskite-type $LaNiO_3$[27,28,32]. Meanwhile, these catalysts also acted as a promoter to enhance the surface transport of Li_xO_2 species by reducing their bonding strength with cathode materials in the discharge and charge process. This can largely faciliate the mass transport for both OR and OE[36,39]. In addition, the porous structure of the nanocubes benefited the fast and uniform diffusion of O_2 and hence resulted in the uniform deposition and distribution of the discharge products (Fig. S3), thereby leading to the decomposition of the discharge products with low overpotential[42].

Although porous $LaNiO_3$ nanocubes showed good ORR and OER performance, it was found that the Li-O_2 battery cell suffered serious capacity fading during the full capacity discharge-charge tests. As can
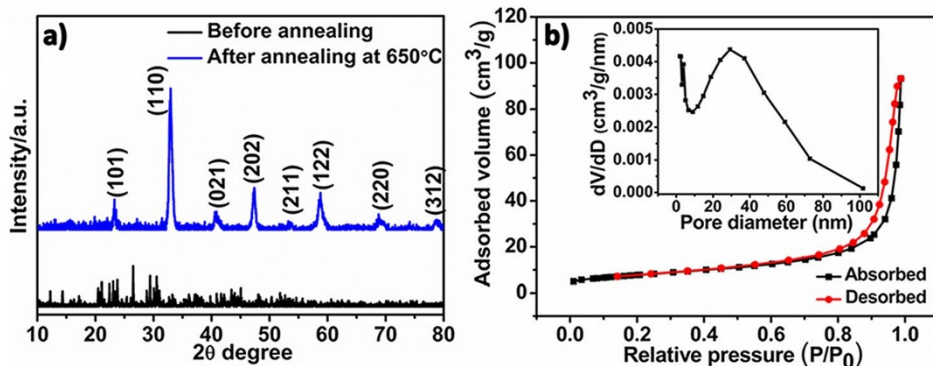
Figure 2 | (a) XRD pattern of the nanocube-like precursors before(black) and after (blue) annealing; (b)Nitrogen adsorption-desorption isotherms and pore size distribution (inset) of porous $LaNiO_3$ nanocubes catalyst.

be seen in Fig. 4a, only 50% capacity was retained after 3 discharge-charge cycles. The serious capacity decay was usually ascribed to the electrode passivation, caused by partial blocking of active sites and pores by undecomposed Li_2O_2 and side products Li_2CO_3 during the discharge-charge cycles[37,43–45]. Interestingly, we also observed serious degradation at the Li anode. After 3 discharge-charge cycles the surface of the Li anode changed from metallic chip to white powders (Fig. S4), which was evidenced to be LiOH by the XRD measurement (Fig. 4b). The formation of LiOH coated on the anode can affect the cycle performance of the battery cell.

To explore the origin of the capacity decay,Raman spectroscopy, XRD and SEM measurements were conducted to analyze the cathode at different discharge-charge states. After 1st discharge, the discharge products coated on the surface of cathode homogeneously, as revealed by SEM image in Fig. 5c. These discharge products were evidenced to be Li_2O_2 based on the XRD pattern and Raman spectra

(Fig. 5a and 5b)[47,48,49]. After charge, the Li_2O_2 related peaks disappeared from the XRD pattern and Raman spectra (Fig. 5a and 5b), indicating that all Li_2O_2 was decomposed without any obvious Li_2O_2 residual. The morphology of the cathode surface after the 1st charge process (Fig. 5d) almost resembled that of the pristine electrode (Fig. S5), further confirming the complete decomposition of Li_2O_2 during the charge process. Similar trend was also observed by XRD and SEM measurement after the 3rd discharge-charge cycle (Fig. 5a, 5e and 5f). However, a weak Li_2CO_3 peak was observed in the Raman spectra after 3rd cycle (Fig. 5b). The Li_2CO_3 was proposed to originate from the unavoidable decomposition of electrolyte and unstable carbon components[50,51]. These Li_2CO_3 could block the small pores in the cathode, which can cause the cathode passivation and result in the capacity fading.

It was also found that the widely used polypropylene (PP) separators could not effectively prevent O_2 diffusion to the Li anode, due to
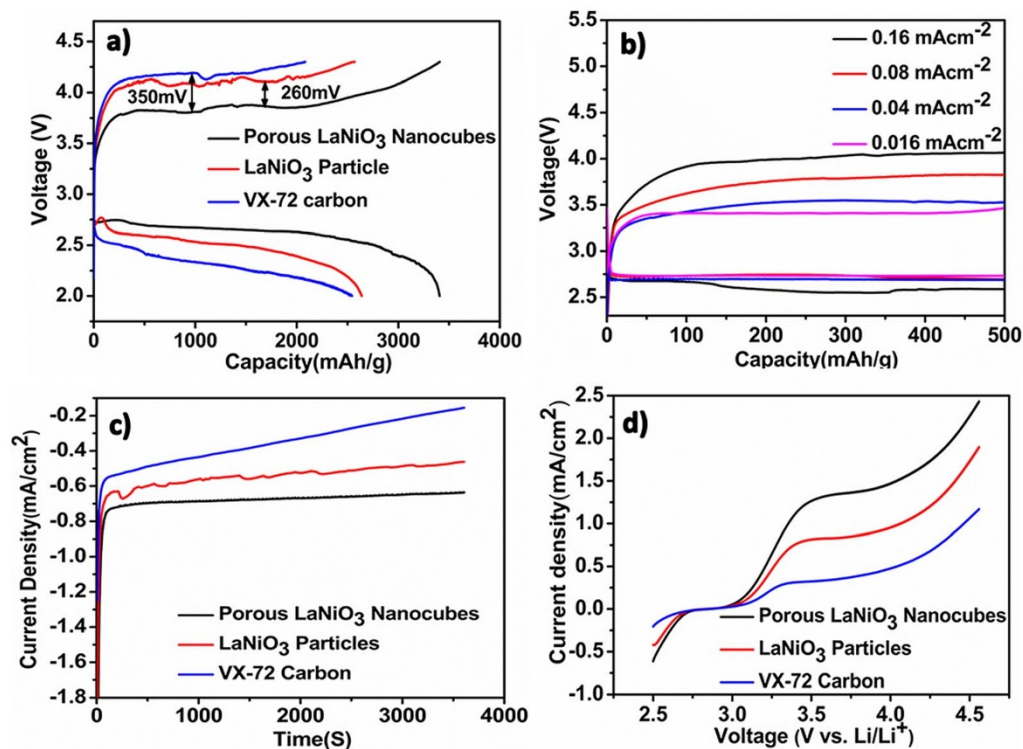

Figure 3 | (a) First discharge-charge curves of Li-O_2 batteries with porous $LaNiO_3$ nanocubes, $LaNiO_3$ particles and VX-72 carbon electrodes at 0.08 mA cm^{-2}; (b) First discharge-charge curves of Li-O_2 battery with porous $LaNiO_3$ nanocubes electrode at 0.16, 0.08, 0.04 and 0.016 mA cm^{-2}; (c) Chronoamperometry showing normalized current evolution with time for various catalysts at 2.25 V; (d) Linear sweep voltammetry of porous $LaNiO_3$ nanocubes, $LaNiO_3$ particles and Vulcan X72 carbon catalysts.
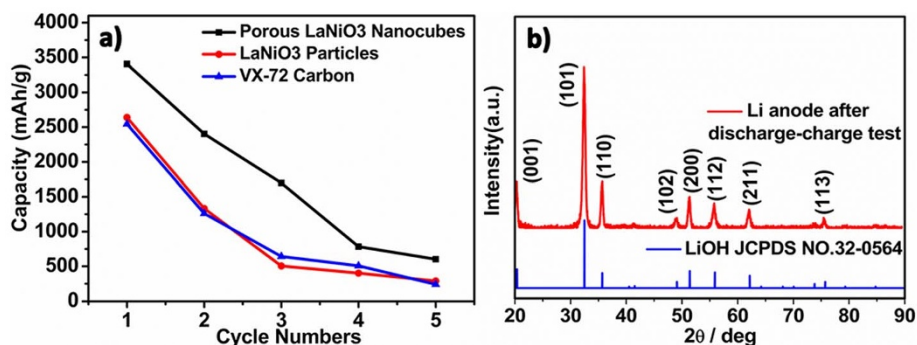
Figure 4 | (a) Discharge capacity with cycle numbers under full capacity discharge-charge test at the current density of 0.08 mA cm^{-2}; b) XRD pattern of the lithium anode after 3 discharge-charge cycles.

their large pore size (Fig. S6). Such oxygen crossover through the separators can promote the decomposition of electrolyte to form hydroxide and then react with lithium cations to form LiOH layer[46]. The trace amount of water diffused from the air and the moisture possibly existed in the electrolyte could also induce the formation of

LiOH at the Li anode. The coating of the indecomposable LiOH on Li anode could greatly inhibit the discharge reaction[52]. Hence, the battery capacity fading was also caused by the incomplete recovery of the lithium anode during the charge process and the continuous consumption of Li by the formation of the indecomposable LiOH during
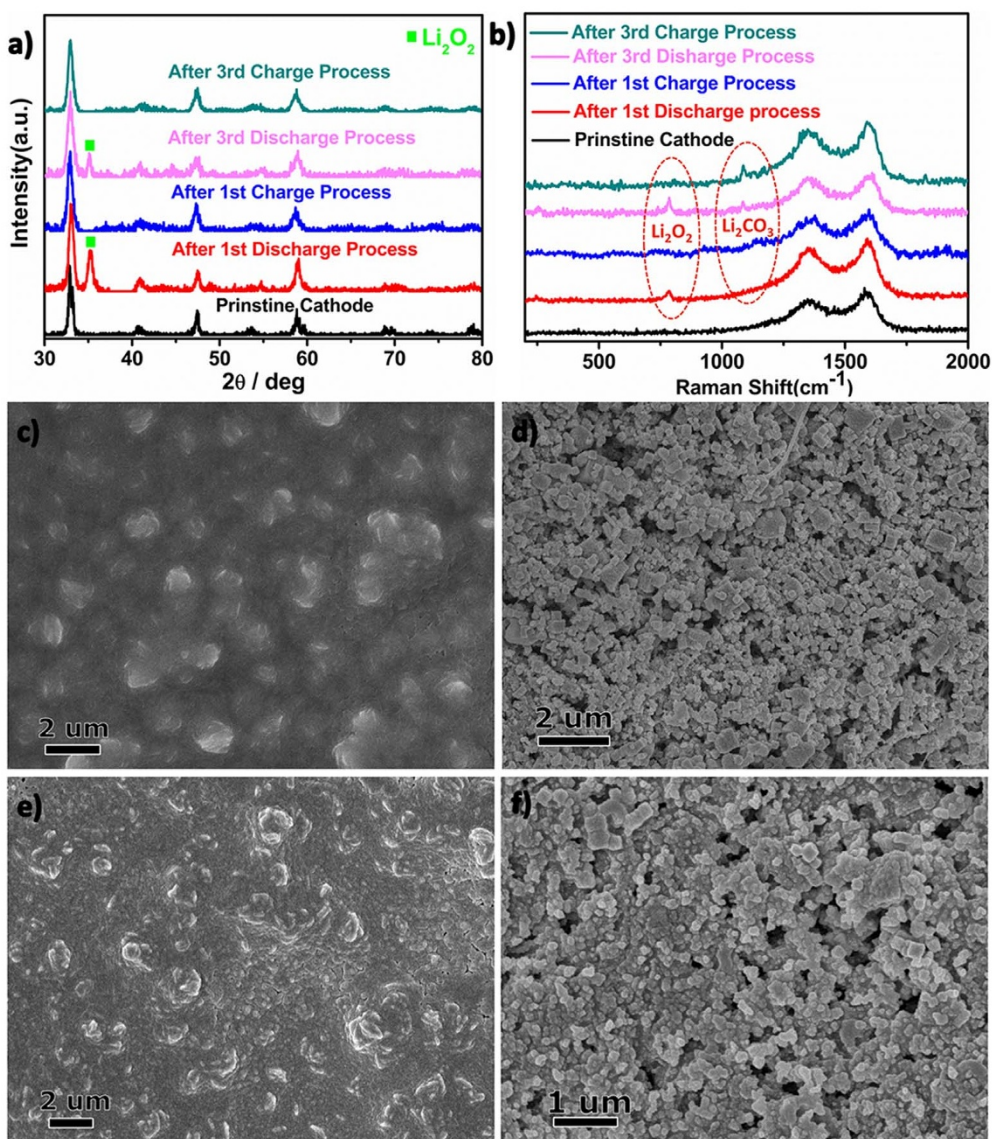

Figure 5 | (a) XRD pattern of the electrodes at different states of discharge and charge; (b) Raman spectra of electrodes at different states of discharge and charge; SEM images of the cathode electrode after (c)1st discharge, (d)1st charge, (e)3rd discharge and (f)3rd charge, respectively.
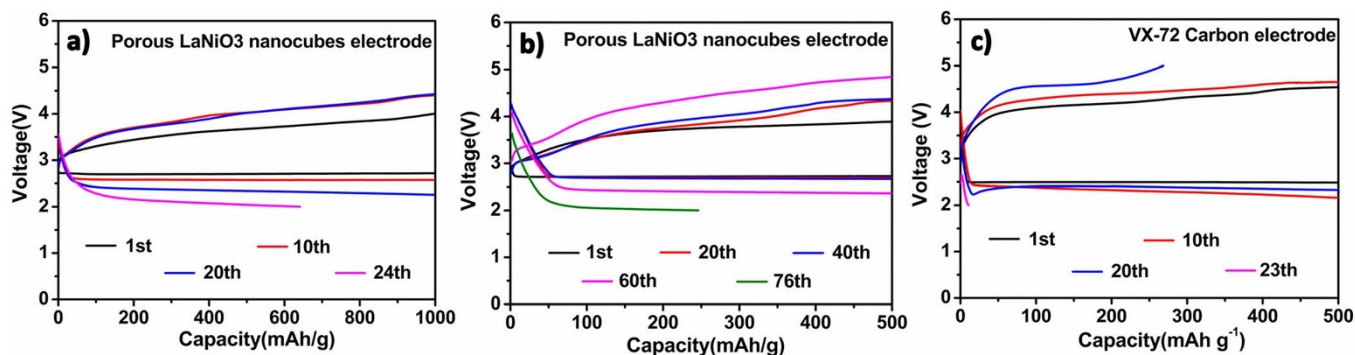
Figure 6 | (a), (b) Cyclic performance of porous LaNiO₃ nanocubes electrode at 0.08 mA cm⁻² with limited capacity of 1000 mAh g⁻¹ and 500 mAh g⁻¹, respectively; (c) Cyclic performance of VX-72 carbon electrode at 0.08 mA cm⁻² with limited capacity of 500 mAh g⁻¹.

the cycles. When "rebuilt" the battery cell by replacing the faded Li electrode with a fresh Li anode, an increased discharge capacity about 1500 mAh g⁻¹ was obtained (Fig. S7). This result further confirmed that the capacity decay was partly originated from the corrosion of Li anode.

To minimize the side effects caused by anode corrosion and cathode passivation, we measured the Li-O₂ battery cell with porous LaNiO₃ nanocubes electrode following a recently widely adoped method[53,54] by limiting the depth of discharge and "rebuilt" the cell with fresh Li metals during the test process. Improved cycle performance of Li-O₂ battery was obtained. Fig. 6a shows the voltage profiles of porous LaNiO₃ nanocubes electrode cycled at 0.08 mA cm⁻² with the curtailing capacity of 1000 mAh g⁻¹. The discharge-charge cycling was carried out for 23 cycles without obvious capacity fading (Fig. 6a). Reducing the curtailing capacity to 500 mAh g⁻¹, the cycle number of the battery could increase to 75 cycles (Fig. 6b), which was much larger than that of VX-72 carbon electrode with 22 cycles under the same condition (Fig. 6c). These results indicate that the porous LaNiO₃ nanocubes electrodes have good rechargeability and cyclability.

In summary, porous LaNiO₃ nanocubes with large specific surface area were employed as cathode catalyst for Li-O₂ battery. The battery assembled with porous LaNiO₃ nanocubes electrode showed excellent charging performance with significantly reduced overpotentials (3.40 V). It also showed enhanced capacity of 3407 mAh g⁻¹ and good cycle stability of 75 cycles without any obvious capacity decay at a 500 mAh g⁻¹ capacity limitation. It was also found that the lithium anode corrosion and cathode passivation were responsible for the capacity fading of Li-O₂ battery. This work suggests an alternative approach to develop high performance catalysts in Li-O₂ battery by tuning the structure of perovskite oxides.

Methods

Synthesis of porous LaNiO₃ nanocubes and LaNiO₃ particles. Typically, 0.455 g La(NO₃)₃, 0.305 g Ni(NO₃)₂·6H₂O and 0.394 g glycine were dissolved in 75 ml deionized (DI) water to form a transparent solution. The pH of the solution was then adjusted to about 7.7 by slowly adding NH₃·H₂O. After 10 min stirring, the solution was transferred into a 90 ml Teflon-lined stainless-steel autoclave and heated at 180 °C for 12 h. The obtained precursors were washed several times and dried at 80 °C. After that, the precursors were annealed at 650 °C for 2 h in O₂ atmosphere to obtain porous LaNiO₃ nanocubes. The reference LaNiO₃ particles were synthesized with the same procedure without using glycine in the hydrothermal reaction system.

Characterizations. The morphology and structure of the catalyst were characterized by SEM on JEOL JSM6700F and TEM on JEOL 3010, respectively. XRD patterns of the catalysts were recorded from a PANalytical Empyren DY 708 diffractometer with Cu radiation (Cu Kα=0.15406 nm). BET surface area was measured by nitrogen sorption at 77 K on a surface area analyzer (QuadraSorb SI). Raman spectroscopy was carried out by the Renishaw Invia system with a 532 nm excitation line. The electrodes were washed with CH₃CN in glove box before the ex-situ SEM, XRD and Raman spectroscopy analysis.

Li-O₂ cell assembly. The oxygen cathodes were prepared by coating the catalyst slurry on carbon paper homogenously. The catalyst slurry was prepared by mixing 40% porous LaNiO₃ nanocubes or LaNiO₃ particles catalysts with 50% VX-72 carbon and 10% polyvinylidene fluoride (PVDF), or 90% VC-72 carbon with 10% PVDF. The geometric area of the electrode was about 1.25 cm² and the mass loading of the catalyst slurry on the electrode was about 1 mg cm⁻². The capacity was calculated based on the total weight of electrode. All Li-O₂ batteries were assembled using modified Swagelok cells in glove box under Argon atmosphere. The cell consisted of a lithium chip as the anode, polypropylene (PP) membrane as the separator and an as-prepared oxygen cathode. 1 M lithium trifluoromethanesulfonate/tretraethylene glycol dimethyl ether (LiCF₃SO₃/TEGDME) was used as the electrolyte. The galvanostatic discharge-charge test was conducted within a voltage window of 2.0–4.3 V (vs. Li/Li⁺).

Rotating disk electrode (RDE) measurement in non-aqueous electrolyte. The catalyst ink was prepared by homogeneously dispersing 3 mg porous LaNiO₃ nanocubes catalysts, 4.5 mg VX-72 carbon into 60 μl Nafion and 600 μl DI water solution. The thin-film electrode was then prepared by drop-casting the catalyst ink onto the flat GC electrode, yielding carbon loading of 0.3 mg₍carbon₎ cm⁻²₍disk₎. The RDE measurement system in non-aqueous electrolyte included a lithium-foil as the counter electrode, a reference electrode and a thin-film working electrode. The reference electrode was a silver wire immersing into 0.1 M tetrabutylammonium hexafluorophosphate (TBAPF₆) and 0.01 M AgNO₃ in TEGDME. Before using it was calibrated against Li metal in 1 M LiCF₃SO₃ TEGDME [0 V (vs. Li/Li⁺) ≈ −3.53 ± 0.01V (vs. Ag/Ag⁺)]. Prior to each experiment, the sealed test system was first purged with Ar for 15 mins, then the working electrode was cycled in Ar [3.4-2 V (vs. Li/Li⁺) at 100 rpm] until a stable cyclic voltammetric profile was obtained. Subsequently, the solution was purged with O₂ for 30 mins for the chronoampperpmmetry studies, by holding the voltage at 2.25 V for 1 h to deposit Li₂O₂. Linear sweep voltammetry (LSV) measurement was conducted with potential scanning from 2.5 to 4.5 V (vs. Li/Li+) with the scan rate of 10 mV S⁻¹.

1. Bruce, P. G., Freunberger, S. A., Hardwick, L. J. & Tarascon, J.-M. Li-O₂ and Li-S batteries with high energy storage. *Nat. Mater.* **11**, 19–29 (2012).
2. Cheng, F. & Chen, J. Metal-air batteries: from oxygen reduction electrochemistry to cathode catalysts. *Chem. Soc. Rev.* **41**, 2172–2192 (2012).
3. Kraytsberg, A. & Ein-Eli, Y. Review on Li–air batteries—Opportunities, limitations and perspective. *J. Power Sources* **196**, 886–893 (2011).
4. Lee, J.-S. *et al.* Metal–Air Batteries with High Energy Density: Li–Air versus Zn–Air. *Adv. Energy Mater.* **1**, 34–50 (2011).
5. Yang, X.-H. & Xia, Y.-Y. The effect of oxygen pressures on the electrochemical profile of lithium/oxygen battery. *J. Solid State Electrochem.* **14**, 109–114 (2010).
6. Yang, X.-H., He, P. & Xia, Y.-Y. Preparation of mesocellular carbon foam and its application for lithium/oxygen battery. *Electrochem. Commun.* **11**, 1127–1130 (2009).
7. Wen, R. & Byon, H. R. In situ monitoring of the Li-O2 electrochemical reaction on nanoporous gold using electrochemical AFM. *Chem. Commun.* **50**, 2628–2631 (2014).
8. Shao, Y., Park, S., Xiao, J., Zhang, J.-G., Wang, Y. & Liu, J. Electrocatalysts for Nonaqueous Lithium–Air Batteries: Status, Challenges, and Perspective. *ACS Catal.* **2**, 844–857 (2012).
9. Hammes-Schiffer, S. Theory of Proton-Coupled Electron Transfer in Energy Conversion Processes. *Acc. Chem. Res.* **42**, 1881–1889 (2009).
10. McCloskey, B. D. *et al.* Limitations in Rechargeability of Li-O2Batteries and Possible Origins. *J. Phys. Chem. Lett.* **3**, 3043–3047 (2012).
11. Wang, J., Li, Y. & Sun, X. Challenges and opportunities of nanostructured materials for aprotic rechargeable lithium–air batteries. *Nano Energy* **2**, 443–467 (2013).

12. Ogasawara, T, Débart, A., Holzapfel, M., Novák, P. & Bruce, P. G. Rechargeable Li2O2 Electrode for Lithium Batteries. *J. Am. Chem. Soc.* **128**, 1390–1393 (2006).

13. Kim, B. G. *et al.* Improved reversibility in lithium-oxygen battery: Understanding elementary reactions and surface charge engineering of metal alloy catalyst. *Sci. Rep.* **4**, (2014).

14. Lei, Y. *et al.* Synthesis of Porous Carbon Supported Palladium Nanoparticle Catalysts by Atomic Layer Deposition: Application for Rechargeable Lithium–O2 Battery. *Nano Lett.* **13**, 4182–4189 (2013).

15. Sun, B., Munroe, P. & Wang, G. Ruthenium nanocrystals as cathode catalysts for lithium-oxygen batteries with a superior performance. *Sci. Rep.* **3**, (2013).

16. Débart, A., Paterson, A. J., Bao, J. & Bruce, P. G. α-MnO2 Nanowires: A Catalyst for the O2 Electrode in Rechargeable Lithium Batteries. *Angew. Chem. Int. Ed.* **47**, 4521–4524 (2008).

17. Zhang, L. *et al.* Mesoporous NiCo2O4 nanoflakes as electrocatalysts for rechargeable Li-O2 batteries. *Chem. Commun.* **49**, 3540–3542 (2013).

18. Cui, Y., Wen, Z. & Liu, Y. A free-standing-type design for cathodes of rechargeable Li-O2 batteries. *Energy Environ. Sci.* **4**, 4727–4734 (2011).

19. Oh, S. H., Black, R., Pomerantseva, E., Lee, J. H. & Nazar, L. F. Synthesis of a metallic mesoporous pyrochlore as a catalyst for lithium-O2 batteries. *Nat. Chem.* **4**, 1004–1010 (2012).

20. Cheng, F., Shen, J., Peng, B., Pan, Y., Tao, Z. & Chen, J. Rapid room-temperature synthesis of nanocrystalline spinels as oxygen reduction and evolution electrocatalysts. *Nat. Chem.* **3**, 79–84 (2011).

21. Oh, S. H. & Nazar, L. F. Oxide Catalysts for Rechargeable High-Capacity Li–O2 Batteries. *Adv. Energy Mater.* **2**, 903–910 (2012).

22. Yilmaz, E., Yogi, C., Yamanaka, K., Ohta, T. & Byon, H. R. Promoting Formation of Noncrystalline Li2O2 in the Li–O2 Battery with RuO2 Nanoparticles. *Nano Lett.* **13**, 4679–4684 (2013).

23. Neburchilov, V., Wang, H., Martin, J. J. & Qu, W. A review on air cathodes for zinc–air fuel cells. *J. Power Sources* **195**, 1271–1291 (2010).

24. Jung, K.-N., Lee, J.-I., Im, W. B., Yoon, S., Shin, K.-H. & Lee, J.-W. Promoting Li2O2 oxidation by an La1.7Ca0.3Ni0.75Cu0.25O4 layered perovskite in lithium-oxygen batteries. *Chem. Commun.* **48**, 9406–9408 (2012).

25. Fu, Z., Lin, X., Huang, T. & Yu, A. Nano-sized La0.8Sr0.2MnO3 as oxygen reduction catalyst in nonaqueous Li/O2 batteries. *J. Solid State Electrochem* **16**, 1447–1452 (2012).

26. Ohkuma, H., Uechi, I., Imanishi, N., Hirano, A., Takeda, Y. & Yamamoto, O. Carbon electrode with perovskite-oxide catalyst for aqueous electrolyte lithium-air secondary batteries. *J. Power Sources* **223**, 319–324 (2013).

27. Yuasa, M., Imamura, H., Nishida, M., Kida, T. & Shimanoe, K. Preparation of nano-LaNiO3 support electrode for rechargeable metal-air batteries. *Electrochem. Commun.* **24**, 50–52 (2012).

28. Yuasa, M., Nishida, M., Kida, T., Yamazoe, N. & Shimanoe, K. Bi-Functional Oxygen Electrodes Using LaMnO3/LaNiO3 for Rechargeable Metal-Air Batteries. *J. Electrochem. Soc.* **158**, A605–A610 (2011).

29. Zhao, Y. *et al.* Hierarchical mesoporous perovskite La0.5Sr0.5CoO2.91 nanowires with ultrahigh capacity for Li-air batteries. *Proc. Natl. Acad. Sci.* **109**, 19569–19574 (2012).

30. Xu, J.-J., Xu, D., Wang, Z.-L., Wang, H.-G., Zhang, L.-L. & Zhang, X.-B. Synthesis of Perovskite-Based Porous La0.75Sr0.25MnO3 Nanotubes as a Highly Efficient Electrocatalyst for Rechargeable Lithium–Oxygen Batteries. *Angew. Chem. Int. Ed.* **52**, 3887–3890 (2013).

31. Suntivich, J., Gasteiger, H. A., Yabuuchi, N., Nakanishi, H., Goodenough, J. B. & Shao-Horn, Y. Design principles for oxygen-reduction activity on perovskite oxide catalysts for fuel cells and metal-air batteries. *Nat. Chem.* **3**, 546–550 (2011).

32. Suntivich, J., May, K. J., Gasteiger, H. A., Goodenough, J. B. & Yang, S. H. A Perovskite Oxide Optimized for Oxygen Evolution Catalysis from Molecular Orbital Principles. *Science* **334**, 1383–1385 (2011).

33. Yu, N., Kuai, L., Wang, Q. & Geng, B. Pt nanoparticles residing in the pores of porous LaNiO3 nanocubes as high-efficiency electrocatalyst for direct methanol fuel cells. *Nanoscale* **4**, 5386–5393 (2012).

34. Tao, A. R., Habas, S. & Yang, P. Shape Control of Colloidal Metal Nanocrystals. *Small* **4**, 310–325 (2008).

35. Peng, T., Yang, H., Pu, X., Hu, B., Jiang, Z. & Yan, C. Combustion synthesis and photoluminescence of SrAl2O4:Eu,Dy phosphor nanoparticles. *Mater. Lett.* **58**, 352–356 (2004).

36. Black, R., Lee, J.-H., Adams, B., Mims, C. A. & Nazar, L. F. The Role of Catalysts and Peroxide Oxidation in Lithium–Oxygen Batteries. *Angew. Chem. Int. Ed.* **52**, 392–396 (2013).

37. Qin, Y. *et al.* In situ fabrication of porous-carbon-supported [small alpha]-MnO2 nanorods at room temperature: application for rechargeable Li-O2 batteries. *Energy Environ. Sci.* **6**, 519–531 (2013).

38. Trahey, L. *et al.* Synthesis, Characterization, and Structural Modeling of High-Capacity, Dual Functioning MnO2 Electrode/Electrocatalysts for Li-O2 Cells. *Adv. Energy Mater.* **3**, 75–84 (2013).

39. Cui, Z. H. & Guo, X. X. Manganese monoxide nanoparticles adhered to mesoporous nitrogen-doped carbons for nonaqueous lithium–oxygen batteries. *J. Power Sources* **267**, 20–25 (2014).

40. McCloskey, B. D., Scheffler, R., Speidel, A., Bethune, D. S., Shelby, R. M. & Luntz, A. C. On the Efficacy of Electrocatalysis in Nonaqueous Li-O2 Batteries. *J. Am. Chem. Soc.* **133**, 18038–18041 (2011).

41. Fan, W., Guo, X., Xiao, D. & Gu, L. Influence of Gold Nanoparticles Anchored to Carbon Nanotubes on Formation and Decomposition of Li2O2 in Nonaqueous Li–O2 Batteries. *J. Phys. Chem. C* **118**, 7344–7350 (2014).

42. Adams, B. D., Radtke, C., Black, R., Trudeau, M. L., Zaghib, K. & Nazar, L. F. Current density dependence of peroxide formation in the Li-O2 battery and its effect on charge. *Energy Environ. Sci.* **6**, 1772–1778 (2013).

43. Younesi, R., Hahlin, M., Björefors, F., Johansson, P. & Edström, K. Li–O2 Battery Degradation by Lithium Peroxide (Li2O2): A Model Study. *Chem. Mater.* **25**, 77–84 (2012).

44. Black, R., Oh, S. H., Lee, J.-H., Yim, T., Adams, B. & Nazar, L. F. Screening for Superoxide Reactivity in Li-O2 Batteries: Effect on Li2O2/LiOH Crystallization. *J. Am. Chem. Soc.* **134**, 2902–2905 (2012).

45. McCloskey, B. D. *et al.* Twin Problems of Interfacial Carbonate Formation in Nonaqueous Li–O2 Batteries. *J Phys Chem. Lett.* **3**, 997–1001 (2012).

46. Assary, R. S. *et al.* The Effect of Oxygen Crossover on the Anode of a Li–O2 Battery using an Ether-Based Solvent: Insights from Experimental and Computational Studies *Chem. Sus. Chem.* **6**, 51–55 (2013).

47. McCloskey, B. D., Bethune, D. S., Shelby, R. M., Girishkumar, G. & Luntz, A. C. Solvents' Critical Role in Nonaqueous Lithium–Oxygen Battery Electrochemistry. *J. Phys. Chem. Lett.* **2**, 1161–1166 (2011).

48. Peng, Z., Freunberger, S. A., Chen, Y. & Bruce, P. G. A Reversible and Higher-Rate Li-O2 Battery. *Science* **337**, 563–566 (2012).

49. Lim, H., Yilmaz, E. & Byon, H. R. Real-Time XRD Studies of Li–O2 Electrochemical Reaction in Nonaqueous Lithium–Oxygen Battery. *J. Phys. Chem. Lett.* **3**, 3210–3215 (2012).

50. Ottakam Thotiyl, M. M., Freunberger, S. A., Peng, Z. & Bruce, P. G. The Carbon Electrode in Nonaqueous Li–O2 Cells. *J. Am. Chem. Soc.* **135**, 494–500 (2012).

51. Xu, W. *et al.* The stability of organic solvents and carbon electrode in nonaqueous Li-O2 batteries. *J Power Sources* **215**, 240–247 (2012).

52. Shui, J.-L. *et al.* Reversibility of anodic lithium in rechargeable lithium–oxygen batteries. *Nat. Commun.* **4**, (2013).

53. Hung, L.-I., Tsung, C.-K., Huang, W. & Yang, P. Room-Temperature Formation of Hollow Cu2O Nanoparticles. *Adv. Mater.* **22**, 1910–1914 (2010).

54. Xu, D., Wang, Z.-L., Xu, J.-J., Zhang, L.-L. & Zhang, X.-B. Novel DMSO-based electrolyte for high performance rechargeable Li-O2 batteries. *Chem. Commun.* **48**, 6948–6950 (2012).

Acknowledgments

Author contributions

J.Z. and W.C. designed the experiments. J.Z. performed the experiments. Y.B.Z. and X.Z. discussed and commented on the experiments and results. J.Z., Z.L.L. and W.C. discussed and wrote the paper.

Additional information